Generation of microwave fields in cavities with laser-excited nonlinear media: competition between the second- and third-order optical nonlinearities

Generation of microwave fields in cavities with laser-excited nonlinear media: competition between the second- and third-order optical nonlinearities

C Braggio, G Carugno

Dip. di Fisica e Astronomia and INFN Sez. di Padova, Via F. Marzolo 8, I-35131 Padova, Italy

E-mail: caterina.braggio@unipd.it

A F Borghesani

CNISM, Dipartimento di Fisica e Astronomia and INFN Sez. di Padova, via F. Marzolo 8, I-35131 Padova, Italy

V V Dodonov

Institute of Physics and International Center for Physics, University of Brasilia, 70910-900, Brasilia, Federal District, Brazil

E-mail: vdodonov@fis.unb.br

F Pirzio

Dip. di Elettronica, Univ. di Pavia, Via Ferrata 1, I-27100 Pavia, Italy

G Ruoso

INFN, Laboratori Nazionali di Legnaro, Viale dell'Università 2, I-35020 Legnaro, Italy

Submitted to: *J. Opt.*

Abstract. We discuss a scheme for parametric amplification of the quantum fluctuations of the electromagnetic vacuum in a three-dimensional microwave resonator and report preliminary measurements to test its feasibility. In the present experimental scheme, the fundamental mode of a microwave cavity is non-adiabatically perturbed by modulating the index of refraction of a nonlinear optical crystal enclosed therein. Intense, multi-GHz laser pulses as those delivered by a mode-locked laser source impinge on the crystal to accomplish the n-index modulation. We theoretically analyze the process of parametric generation, which is related to the third-order nonlinear coefficient $\chi^{(3)}$ of the nonlinear crystal, and assess suitable experimental conditions for generating real photons from the vacuum. Second-order nonlinear processes are first analyzed as possible source of spurious photons in quantum vacuum experiments when an *ideal*, mode-locked laser source is considered. The combination of a crystal non-null $\chi^{(2)}$ coefficient and a *real* mode-locked laser system, i.e. featuring offset-from-carrier noise and unwanted secondary oscillations, is also experimentally investigated in the second part of the work, paving the way for future experiments in three-dimensional cavities.

PACS numbers: 42.50.Pq, 42.65.-k, 42.65.Yj

23 March 2018

1. Introduction

Illuminating a nonlinear crystal with a powerful laser beam, one can change the refractive index of the sample. A modulation of the laser beam intensity results in a time variation of the refractive index. If the crystal is put inside an electromagnetic cavity, the time variation of the refractive index can be interpreted as a time variation of the optical length of the cavity. Hence, this arrangement can be used for studies of the so called Dynamical Casimir Effect (DCE) – an intriguing prediction of the quantum theory that photons could be generated from the quantum vacuum state in cavities with moving boundaries (see [1–3] for the most recent reviews). Such ideas were discussed for a long time by many authors [4–13].

We consider a possibility of DCE in a microwave cavity, enclosing a nonlinear crystal, whose refractive index is modulated by near infrared (NIR) high-intensity laser pulses. A preliminary analysis made in [14] showed that such a scheme could be feasible for crystals possessing sufficiently big *third-order* nonlinear susceptibility coefficients $\chi^{(3)}$. However, real crystals possess also the *second-order* nonlinear susceptibility coefficients $\chi^{(2)}$. Although it is known that $\chi^{(2)}$ must be zero in crystals possessing the inversion symmetry [15], this is true, as a matter of fact, in the idealized case of *infinite ideal* crystals, whereas real crystals of finite size do show the second-order nonlinear effects, either due to the presence of some impurities/defects or due to the loss of the inversion symmetry in the regions nearby the surface [16–20]. The generation of microwave radiation in the cavity containing different nonlinear materials with high $\chi^{(2)}$ coefficients, irradiated with intense infra-red pulse trains, was reported in [21, 22]. Although this phenomenon can find various useful applications, it should be considered as a spurious effect in the DCE experiments, because the related mechanism can be considered as totally *classical*, i.e. having nothing in common with the existence and amplification of *quantum* fluctuations of the electromagnetic field. This will be shown in section 2.4. Therefore one of our main objectives is to evaluate, how strong this spurious effect could be in experiments with real third-order nonlinear crystals. This is the subject of section 2.

The second part of the paper is devoted to a feasibility study, in which we experimentally investigate the limitations related to the utilization of the laser system that allows repetition rates as high as those requested in the DCE experiment (multi-GHz repetition rates), the mode-locked laser. Moreover, we systematically study the phenomenon of direct microwave generation related to the utilization of a nonlinear crystal endowed also by a $\chi^{(2)}$ coefficient.

2. Theoretical model

Since variations of the refractive index are very small (due to the smallness of the nonlinear coefficients $\chi^{(3)}$), the cavity design is dictated by the necessity to reach a maximal sensitivity of cavity eigenfrequencies to these small variations. This can be achieved in a reentrant cavity, shown in Fig. 1. The main part of the gap

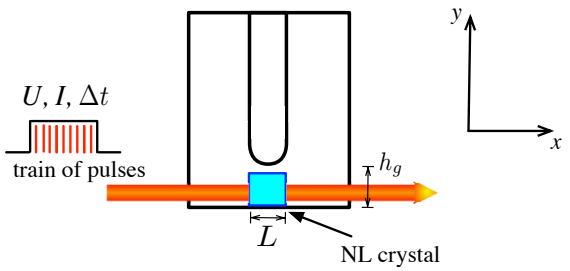

Figure 1. The theoretical problem we consider: a reentrant microwave cavity is perturbed by laser pulses impinging on a nonlinear crystal that is placed in the gap region. The length of the crystal along the laser propagation direction x is L and h_g is the height of the gap. The train of pulses lasts T_t and its energy is U.

between the flat base and the cylindrical post is filled in with a nonlinear dielectric material (crystal). We assume that the electric field in the fundamental cavity mode is almost uniform inside the gap. This crystal is periodically illuminated with intense laser micro pulses of a few picosecond duration, within a macro pulse of total duration about a few microsecond. The change of refractive index of the crystal due to the $\chi^{(3)}$ nonlinear coefficient leads to periodical changes of the instantaneous cavity eigenfrequency. These periodical variations, in turn, should result in the generation of microwave quanta from the initial vacuum state. In this section we give the theoretical description of this effect, showing that the number of generated quanta depends on the total energy of the macropulse. We also discuss how to diminish spurious effects due to the imminent presence of $\chi^{(2)}$ nonlinearities.

2.1. Basic field equations

We start with the Maxwell equations in the CGS units

$$\mathrm{rot}\mathbf{E} = -\frac{1}{c}\frac{\partial \mathbf{B}}{\partial t}, \tag{1}$$

$$\mathrm{rot}\mathbf{H} = \frac{1}{c}\frac{\partial \mathbf{D}}{\partial t} = \frac{\varepsilon(\mathbf{r})}{c}\frac{\partial \mathbf{E}}{\partial t} + \frac{4\pi}{c}\frac{\partial \mathbf{P^{NL}}}{\partial t}. \tag{2}$$

The form of the second equation means that we neglect the frequency dependence of the dielectric permeability. Consequently, this is a simplified model. Another assumption is that the nonlinear part of the

polarization vector $\mathbf{P^{NL}}(t)$ depends on the electric field components at the same time instant:

$$P_i^{NL} = \chi_{ijk}^{(2)} E_j E_k + \chi_{ijkl}^{(3)} E_j E_k E_l, \tag{3}$$

where coefficients $\chi_{ijk}^{(2)}$ and $\chi_{ijkl}^{(3)}$ do not depend on time. Here we use the standard notation from [15] and the standard summation rule over repeated indexes. If the electric field amplitude in the laser beam slowly varies with time (in the time scale which is several orders of magnitude bigger than the period of oscillations of the infrared laser light), then vector $\mathbf{P^{NL}}(t)$ contains, besides rapidly oscillating terms, also small terms varying in that long time scale. As a consequence, these terms produce a slowly varying electric field. Therefore we can write the total electric field as the sum of a weak microwave (RF) field $\mathbf{E}^{(R)}$ and a strong near infrared laser field $\mathbf{E}^{(L)}$. Since we are interested here in the dynamics of the field $\mathbf{E}^{(R)}$ (assuming that the time dependence of the laser field is given), we perform *averaging* equations (1)-(3) over time intervals of the order of $10^{-13} - 10^{-12}$ s, which are much longer than the period of oscillations of the laser field, but much shorter than the period of oscillations of the RF field. The RF field components practically do not change after such an averaging. On the other hand, if the laser field is quasi-monochromatic, we may assume that

$$\overline{E_j^{(L)}} = \overline{E_j^{(L)} E_k^{(L)} E_l^{(L)}} = 0, \tag{4}$$

where the bar means the average value. This procedure eliminates the laser field components from equation (1). But these components give contributions to the average nonlinear polarization vector $\mathbf{P^{NL}}$:

$$\overline{P_i^{NL}} = \chi_{ijk}^{(2)} \overline{E_j^{(L)} E_k^{(L)}} + a_{ij} E_j^{(R)}, \tag{5}$$

$$a_{ij} = \overline{E_k^{(L)} E_l^{(L)}} \left(\chi_{ijkl}^{(3)} + \chi_{ikjl}^{(3)} + \chi_{ilkj}^{(3)} \right). \tag{6}$$

We have neglected here small terms proportional to $E_j^{(R)} E_k^{(R)}$ and $E_j^{(R)} E_k^{(R)} E_l^{(R)}$, since the RF field is supposed to be much weaker than the laser one.

We consider the laser beam propagating in the x direction (see Figure 1), whose electric field vector is polarized along the vertical y axis. ‡ For this geometry, the part of the polarization vector arising due to the second order nonlinearity can be written as

$$\overline{\mathbf{P}^{(2)}} = (4\pi/c) \chi_{max}^{(2)}(\mathbf{r}) \mathbf{b}(\mathbf{r}) I(\mathbf{r}; t), \tag{7}$$

where $I = (c/4\pi) \overline{\left[E^{(L)}\right]^2}$ is the time-average Poynting vector of the laser beam, $\chi_{max}^{(2)}(\mathbf{r})$ is the maximal value of coefficients $\chi_{ijk}^{(2)}$ at point $\mathbf{r}$ inside the nonlinear crystal, and vector $\mathbf{b}(\mathbf{r})$ has the following components:

$$b_i(\mathbf{r}) = \chi_{i22}^{(2)}(\mathbf{r}) / \chi_{max}^{(2)}(\mathbf{r}). \tag{8}$$

The tensor a_{ij} defined by equation (6) has the following components in the specific case under consideration:

$$a_{ij} = (4\pi/c) I(\mathbf{r}; t) \left[\chi_{ij22}^{(3)} + \chi_{i2j2}^{(3)} + \chi_{i22j}^{(3)} \right].$$

Neglecting the anisotropy of coefficients $\chi_{ijkl}^{(3)}$, we have $a_{ij} = 0$ if $i \neq j$ [15] . Assuming that $\chi_{ii22}^{(3)} = \chi_{i2i2}^{(3)} = \chi_{i22i}^{(3)} = \chi_{2222}^{(3)} \equiv \chi^{(3)}$, we can rewrite equation (2) as

$$\mathrm{rot}\mathbf{H} = \frac{1}{c} \frac{\partial}{\partial t} \left[\tilde{\varepsilon}(\mathbf{r}; t) \mathbf{E} \right] + \frac{4\pi}{c} \mathbf{J}(\mathbf{r}; t), \tag{9}$$

with

$$\tilde{\varepsilon}(\mathbf{r}; t) = \varepsilon(\mathbf{r}) + 48\pi^2 \chi^{(3)}(\mathbf{r}) I(\mathbf{r}; t), \tag{10}$$

$$\mathbf{J}(\mathbf{r}; t) = (4\pi/c) \chi_{max}^{(2)}(\mathbf{r}) \mathbf{b}(\mathbf{r}) \partial I(\mathbf{r}; t) / \partial t. \tag{11}$$

Hereafter $\mathbf{E}$ and $\mathbf{H}$ in all equations will mean the averaged RF electric and magnetic fields, whereas the laser field will be hidden in the averaged intensity $I(\mathbf{r}; t)$. We see that the third order nonlinearity results in a change of the effective dielectric constant inside the nonlinear crystal, which is proportional to the laser intensity. The second order nonlinearity gives rise to an effective current, which is proportional to the *time derivative* of laser intensity $\partial I / \partial t$.

It is convenient to rewrite equations (1) and (9) in terms of the electric induction vector $\mathbf{D}$ and magnetic field vector $\mathbf{H}$ (assuming $\mathbf{B} = \mathbf{H}$ for non-magnetic media):

$$\mathrm{rot}\left[\mathbf{D} / \tilde{\varepsilon}(\mathbf{r}; t) \right] = -(1/c) \partial \mathbf{H} / \partial t, \tag{12}$$

$$\mathrm{rot}\mathbf{H} = (1/c) \partial \mathbf{D} / \partial t + (4\pi/c) \mathbf{J}(\mathbf{r}; I(\mathbf{r}; t)). \tag{13}$$

Excluding vector $\mathbf{H}$, we arrive at the inhomogeneous second order equation

$$\mathrm{rotrot}\left(\frac{\mathbf{D}}{\tilde{\varepsilon}(\mathbf{r}; t)} \right) = -\frac{1}{c^2} \frac{\partial^2 \mathbf{D}}{\partial t^2} - \frac{4\pi}{c^2} \frac{\partial \mathbf{J}(\mathbf{r}; I(\mathbf{r}; t))}{\partial t}, \tag{14}$$

which contains a source term proportional to the second-order derivative of the averaged laser intensity.

2.2. Reduction to forced nonstationary oscillators

Since the time variable t enters equation (14) through the function $I(\mathbf{r}; t)$ only, we can look for its solutions in the form of the expansion over 'instantaneous' basis

$$\mathbf{D}(\mathbf{r}, t) = \sum_n Q_n(t) \mathbf{D}_n(\mathbf{r}; I), \tag{15}$$

where functions $\mathbf{D}_n(\mathbf{r}; I)$ satisfy the equation

$$\mathrm{rot\ rot}\left(\frac{\mathbf{D}_n(\mathbf{r}; I)}{\tilde{\varepsilon}(\mathbf{r}; I(\mathbf{r}; t))} \right) = \frac{\omega_n^2(I)}{c^2} \mathbf{D}_n(\mathbf{r}; I) \tag{16}$$

‡ Actually, the electric field inside the beam has also a small x component, due to the equation $\mathrm{div}\mathbf{E} = 0$. However, the ratio $|E_x/E_y|$ is of the order of [23] $\lambda z/d^2$, where λ is the laser wavelength, y is the vertical displacement from the beam axis, and d the effective length of the beam. Therefore $|E_x/E_y| \sim \lambda/d \ll 1$ even for $y \sim d$, provided the relation $d \gg \lambda$ is satisfied.

with a 'frozen' function $\tilde{\varepsilon}(\mathbf{r}; I(\mathbf{r};t))$. It is important that functions $\mathbf{D}_n(\mathbf{r};I)$ form a complete orthogonal set with respect to the following scalar product:

$$\int \frac{\mathbf{D}_n(\mathbf{r};I)\mathbf{D}_m(\mathbf{r};I)}{\tilde{\varepsilon}(\mathbf{r};I(\mathbf{r};t))} d^3\mathbf{r} = \delta_{mn}. \tag{17}$$

To obtain equations for coefficients $Q_n(t)$ we put expansion (15) in equation (14) with account of (16), multiply the equation thus obtained by the function $\mathbf{D}_m(\mathbf{r};I)/\tilde{\varepsilon}(\mathbf{r};I(\mathbf{r};t))$ and integrate over the whole cavity volume, using the orthogonality property (17). Writing $\mathbf{D}_n(\mathbf{r};t) = \mathbf{D}_n^{(0)}(\mathbf{r}) + \mathbf{K}_n(\mathbf{r};I)$, where $\mathbf{D}_n^{(0)}(\mathbf{r})$ is the solution to Eq. (16) with time independent function $\varepsilon(\mathbf{r})$ instead of $\tilde{\varepsilon}(\mathbf{r};I(\mathbf{r};t))$ (i.e., without perturbations caused by the laser illumination), we obtain the following set of coupled ordinary differential equations for coefficients $Q_n(t)$:

$$\ddot{Q}_n + \omega_n^2(t)Q_n + \sum_m \left[2\dot{Q}_m G_{mn} + Q_m h_{mn}\right] = F_n,$$

where time-dependent functions $G_{mn}(t)$, $h_{mn}(t)$, and $F_n(t)$ are given by some integrals containing scalar products of functions $\mathbf{D}_n(\mathbf{r};I)$ with time derivatives of functions $\mathbf{K}_m(\mathbf{r};I)$ and $\mathbf{J}(\mathbf{r};I(\mathbf{r};t))$. However, it can be shown that the terms containing small coefficients $G_{mn}(t)$ and $h_{mn}(t)$ can be neglected [14]. § Thus we arrive at the set of uncoupled equations for the forced harmonic oscillators with time-dependent frequencies

$$\ddot{Q}_n + \omega_n^2(t)Q_n = F_n(t), \tag{18}$$

where

$$\frac{F_n(t)}{(4\pi)^2} = -\frac{\int d^3\mathbf{r}\,\chi^{(2)}_{max}\left[\partial^2 I(\mathbf{r};t)/\partial t^2\right]\mathbf{b}(\mathbf{r})\mathbf{E}_n^{(0)}(\mathbf{r})}{c\int d^3\mathbf{r}\,\varepsilon(\mathbf{r})\left[\mathbf{E}_n^{(0)}(\mathbf{r})\right]^2}. \tag{19}$$

It is convenient to normalize the basis functions $\mathbf{D}_n^{(0)}(\mathbf{r}) = \varepsilon(\mathbf{r})\mathbf{E}_n^{(0)}(\mathbf{r})$ in such a way that the total energy of the field equals $\hbar\omega_c$ (formally, 'one photon' inside the cavity). This means that the electric energy equals $\hbar\omega_c/2$, i.e.,

$$\int d^3\mathbf{r}\,\varepsilon(\mathbf{r})\left[\mathbf{E}_n^{(0)}(\mathbf{r})\right]^2 = 4\pi\hbar\omega_c. \tag{20}$$

In such a case, the variable $Q(t)$ is dimensionless, as well as the quantity

$$\mathcal{N} = \frac{1}{2}\left(Q^2 + \dot{Q}^2/\omega_c^2\right), \tag{21}$$

which has the meaning of the number of quanta in the selected field mode (between and after the laser pulses).

§ These terms are important for cavities with *equidistant* frequency spectra [24], but for realistic 3D cavities the intermode coupling is insignificant in the case of parametric resonance, when laser intensity $I(t)$ varies periodically at twice the frequency of some selected mode, as was shown in [25, 26].

2.3. Parametric amplification due to $\chi^{(3)}$ nonlinearity

If $\chi^{(2)} = 0$, then $F(t) \equiv 0$, and we have the problem of parametrically excited oscillator. Here quantum effects of the amplification of the initial vacuum oscillations can manifest themselves. This case have been analyzed already in [14], so that here we bring the main results of that study with some modifications. Considering the excitation of the fundamental cavity mode, we omit hereafter index n in equation (18) and write $\omega(t) = \omega_c\left[1+\beta(t)\right]$, where ω_c is the unperturbed fundamental cavity angular eigenfrequency ($\omega_c = 2\pi f_c$) and the small correction $\beta(t)$ is proportional to the product of $\chi^{(3)}$ and the instantaneous pulse power $P(t)$. Therefore $\beta(t) = 0$ during intervals between the laser pulses.

The maximal number of quanta that could be generated from the initial vacuum quantum state after n pulses equals [27–29]

$$\mathcal{N}_n = \sinh^2(n\nu), \quad \nu = \omega_c\left|\int_0^{t_f}\beta(t)e^{-2i\omega_c t}dt\right|, \tag{22}$$

provided the repetition rate of laser pulses is chosen as

$$f_l = 2f_c(1-\varphi/\pi), \qquad \varphi = -\omega_c\int_0^{t_f}\beta(t)dt. \tag{23}$$

Here we assume that $\beta(t) = 0$ at $t = 0$ and $t = t_f$.

To find the function $\beta(t)$, we use the known formula [30–32] for small variations of the eigenfrequency of an ideal cavity due to small variations of dielectric permeability ε inside the cavity:

$$\frac{\delta\omega}{\omega} \approx -\frac{\int \delta\varepsilon(\mathbf{r})\,\mathbf{E}^2\,dV}{2\int\varepsilon(\mathbf{r})\mathbf{E}^2\,dV}. \tag{24}$$

Here $\mathbf{E}(\mathbf{r})$ is the unperturbed electric field of the chosen resonance mode and $\varepsilon(\mathbf{r})$ is the dielectric function in the unperturbed cavity. Assuming that the electric field is approximately uniform in the gap region of the reentrant cavity hosting the nonlinear crystal, we can write $\beta(t) = RY(t)$, where $Y(t) = \int\delta\varepsilon(\mathbf{r};t)\,dV$. The geometrical coefficient R can be found if the derivative $\partial\omega/\partial\varepsilon$ for the given geometry of cavity and crystal is known (e.g. through numerical simulations). If the perturbation $\delta\varepsilon$ is constant throughout the crystal volume, we can write two equalities: $\beta = R\delta\varepsilon L S_{cr}$ and $\beta = (\partial\omega/\partial\varepsilon)\delta\varepsilon/\omega_c$, where S_{cr} is the crystal cross section area. Consequently, $R = (\partial\omega/\partial\varepsilon)/(\omega_c L S_{cr})$.

For the Kerr type nonlinearity with the refractive index $n = n_0 + n_2 I$ (where $n_2 = 12\pi^2\chi^{(3)}/n_0^2$ [15]) we have $\delta\varepsilon(\mathbf{r};t) = 2n_G n_2 I(\mathbf{r};t)$, where n_G is the refractive index in the microwave domain. If the transverse size of the laser beam is smaller than that of the crystal,

$$Y(t) = \eta\int_0^L dx\int I(\mathbf{r};t)\,dS = \eta\int_0^L dx P(x;t).$$

where $\eta = 2n_G n_2$ and $P(x;t) = \int I(\mathbf{r};t)\,dS$ is the pulse power at point x and instant t. Consequently,

$$\nu = \omega_c\eta RG, \quad G = \left|\int_0^{t_f}dt\int_0^L dx P(x;t)e^{-2i\omega_c t}\right|. \tag{25}$$

Let us consider sharp rectangular laser pulses of duration τ and power P_0. Then function $P(x,t)$ equals P_0 or zero, depending on the relation between τ and the propagation time through the crystal $T_p = L/v_g$, where v_g is the group velocity of the laser pulse. Calculating the integral in (25) we get

$$G = u_p L \left|\mathrm{sinc}\left(\omega_c \tau\right) \mathrm{sinc}\left(\omega_c T_p\right)\right|, \tag{26}$$

where $u_p = P\tau$ is the energy of a single laser pulse and $\mathrm{sinc}(x) \equiv \sin(x)/x$. For short laser pulses ($\omega_c t_f \ll 1$) and short crystals ($\omega_c T_p \ll 1$) we have $G = u_p L$, where $u_p = P t_f$ is the energy of a single pulse. Hence the number of produced RF quanta $\mathcal{N}_n$ depends on the *total energy* of macropulse $U = n u_p$ [14]:

$$\mathcal{N}_n = \sinh^2\left(|n_2| U K\right), \qquad K = \frac{2 n_G}{S_{cr}} \frac{\partial \omega}{\partial \varepsilon}. \tag{27}$$

Equation (27) shows that to generate, say, 10 photons from the vacuum, one needs the product $n_2 U K \approx 2$. One of possible materials with the necessary symmetry and $\chi^{(2)} = 0$ in the bulk could be diamond with $n_2 \approx 10^{-15}\,\mathrm{cm}^2/\mathrm{W}$. For the total energy $U = 1\,\mathrm{J}$, we need $K \approx 2 \times 10^{15}\,\mathrm{s}^{-1}\mathrm{cm}^{-2}$. To evaluate possible realistic values of the coefficient K, we notice that if the gap height h_g is much smaller than the post diameter d, the standard LC-formula for the resonance frequency $\omega = 1/\sqrt{\mathcal{L}C}$ can be used, where $\mathcal{L}$ is the inductance of the cavity and C is the capacitance, approximated by the simple plain capacitor formula. Assuming that the dielectric crystal occupies all the gap, we can write (in the SI units) $C \approx \varepsilon\varepsilon_0 S_{cap}/h_g$, where S_{cap} is the area of the crystal side parallel to the post. The transverse area of crystal is $S_{cr} \approx L_\perp \cdot h_g$, where $L_\perp$ is the crystal width (it is close to the post diameter d). Using the chain of equalities

$$\frac{\partial \omega}{\partial \varepsilon} = -\frac{1}{2}\left(\mathcal{L}C^3\right)^{-1/2} \frac{\partial C}{\partial \varepsilon} = -\frac{\omega}{2C}\frac{C}{\varepsilon} = -\frac{\omega}{2\varepsilon},$$

we get the estimation

$$K \approx \omega/(h_g L_\perp \sqrt{\varepsilon}). \tag{28}$$

The cavity used in the preliminary measurements had $\omega = 1.44 \times 10^{10}\,\mathrm{rad/s}$, $h_g = L_\perp = 3\,\mathrm{mm}$ and $\varepsilon \approx 9$ (a ZnSe crystal in the gap). Then $K \approx 5 \times 10^{10}\,\mathrm{s}^{-1}\mathrm{cm}^{-2}$, which is a very small number. Considering a smaller cavity with the same geometry, we may suppose that the necessary value of coefficient K could be achieved for the cavity scaled by the factor 30 (taking into account that the cavity eigenfrequency scales inversely proportional to the cavity size). This would be a very small cavity, but probably its size could be increased if higher values of the derivative $\partial\omega/\partial\varepsilon$ were found for some more sophisticated design of the cavity geometry.

2.4. Influence of the $\chi^{(2)}$ surface nonlinearity

Although $\chi^{(2)} = 0$ in the bulk part of the ideal diamond crystal, this coefficient is different from zero in a thin region near the surface. We suppose that the laser beam propagates totally inside the crystal, so that only the surfaces $x = x_0$ and $x = x_0 + L$ (perpendicular to the propagation direction) can give a contribution to the vector $\mathbf{P}^{(2)}$ and to the effective 'force' (19) (we omit again the mode index n). Then we can write (following [16])

$$\chi^{(2)}_{max}(\mathbf{r}) = \tilde{\chi}^{(2)}_{max}(x_0, y, z)\delta(x - x_0) + \tilde{\chi}^{(2)}_{max}(x_0 + L, y, z)\delta(x - x_0 - L), \tag{29}$$

where x_0 is left boundary of the crystal.

Let us assume for the sake of simplicity that the cavity mode electric field is uniform in the crystal volume and coefficients $\tilde{\chi}^{(2)}_{max}$ do not depend on their arguments, as well as the dielectric permeability ε inside the crystal and vector $\mathbf{b}$ in equation (7). Then the effective force (19) can be written as

$$F(t) = \tilde{\chi}^{(2)}_{max}\tilde{R}\left[\frac{\partial^2 P}{\partial t^2}(x_0; t) + \frac{\partial^2 P}{\partial t^2}(x_0 + L; t)\right], \tag{30}$$

where

$$\tilde{R} = -\frac{(4\pi)^2\left(\mathbf{b}\cdot\mathbf{E}_{gap}\right)}{c\int \varepsilon \mathbf{E}^2\, dV}, \quad P(x;t) = \int I(x,y,z;t)\, dydz.$$

Note that for the lossless crystal we have

$$P(x_0 + L; t) = P(x_0; t - T_p), \quad T_p = L/v_g. \tag{31}$$

As was shown in the preceding subsection, small time variations of the frequency $\omega(t)$ manifest themselves only after a great number of pulses. On the contrary, the effect of the time dependent force $F(t)$ can be seen already after a few pulses. Therefore it is sufficient to consider the case of $\omega = \omega_c = const$ to estimate the contribution of the second-order surface nonlinearity to the RF field generation in the cavity. This way we arrive at the standard problem of excitation of a harmonic oscillator by an external time dependent force $F(t)$.

It is convenient to introduce the complex amplitude $\xi(t) = \dot{Q} + i\omega_c Q$. Its evolution according to equation (18) is given by the well known formula

$$\xi(t) = e^{-i\omega_c t}\left[\xi_0 + A(t)\right]. \tag{32}$$

The constant amplitude ξ_0 is determined by the initial conditions (e.g., some preloaded field or a thermal stochastic field), whereas

$$A(t) = \int_0^t F(t') e^{i\omega_c t'} dt'. \tag{33}$$

Then the quantity $\mathcal{N}(t)$, defined by equation (21), reads as $\mathcal{N}(t) = |\xi(t)|^2/(2\omega_c^2)$. In particular, in the case of an initial thermal field, the phase of the complex number ξ_0 is random, so that after

averaging over many measurements we have $\langle \mathcal{N}(t) \rangle = \left[|\xi_0|^2 + |A(t)|^2 \right] / (2\omega_c^2)$. We suppose that the laser illumination starts at $t = 0$ and stops at $t = T_f$. To find the final amplitude A_f for $t > T_f$ we put expression (30) into (33) and perform two integrations by parts. Taking into account account (31), we obtain

$$A_f = -\tilde{\chi}^{(2)}_{max} \tilde{R} \omega_c^2 \left(1 + e^{i\omega_c T_p}\right) \int_0^{T_f} P(t) e^{i\omega_c t} dt, \qquad (34)$$

where $P(t)$ is the time dependent power of the laser pulses. After the series of n identical and strictly periodic pulses of duration τ and periodicity T, the standard formula for the 'time diffraction' on n 'time slits' yields

$$|A_n|^2 = |A_1|^2 \left[\frac{\sin\left(n\omega_c T/2\right)}{\sin\left(\omega_c T/2\right)} \right]^2, \qquad (35)$$

where A_1 is given by formula (34) with T_f replaced by the duration of a single 'micropulse' t_f. For short pulses ($\omega_c \tau \ll 1$) and short crystals ($\omega_c T_p \ll 1$) we have $|A_1| = \left| 2\tilde{\chi}^{(2)}_{max} \tilde{R} \right| \omega_c^2 u_p$, independently of the concrete form of function $P(t)$.

The pulse repetition rate in the DCE experiments must be close to the twice cavity frequency, but with some small deviation [27]. Writing $T = (1 + \phi) T_c/2$ with $|\phi| \ll 1$, we can neglect the small phase ϕ in the denominator of fraction in equation (35). Therefore the number of 'spurious' quanta, that can be added to the initial level $|\xi_0|^2/(2\omega_c^2)$ due to the $\chi^{(2)}$ nonlinearity after n laser pulses, can be evaluated as

$$\mathcal{N}^{(2)}_n = 2 \left\{ \tilde{\chi}^{(2)}_{max} \tilde{R} \omega_c u_p \sin\left[n\pi(1 + \phi)/2\right] \right\}^2. \qquad (36)$$

The microwave signal due to the $\chi^{(2)}$ nonlinearity, can thus exhibit some kind of 'beats' with period $\Delta T \approx T_c/\phi$. Actually, the real temporal behavior of the microwave signal can be even more complicated than predicted by this simple model, as shown in section 4.1.

To estimate the number of spurious quanta, we need the value of coefficient $\tilde{R}$, which strongly depends on the mutual orientation of vectors $\mathbf{b}$ and $\mathbf{E}_{gap}$, i.e., on the orientation of the crystal optical axes. We can estimate the maximal possible value $|\tilde{R}|_{max}$ by assuming that the vectors are parallel and that the electric field is concentrated in an 'effective cavity volume' V_c. The cavity field in the gap region can be evaluated from the normalization integral (20): $|\mathbf{E}_{gap}| \approx \sqrt{4\pi\hbar\omega_c/\varepsilon V_c}$, where $V_c = L h_g L_\perp$ is the crystal volume (assuming that the crystal occupies all the gap). Then $|\tilde{R}|_{max} \approx \left[\hbar\omega_c \varepsilon V_c c^2/(4\pi)^3\right]^{-1/2}$. Therefore we obtain for the parallel vectors $\mathbf{b}$ and $\mathbf{E}_{gap}$the following (very rough) estimation:

$$\mathcal{N}^{(2)}_{max} \approx \frac{128\pi^3 \omega_c}{\hbar \varepsilon c^2 V_c} \left(\tilde{\chi}^{(2)}_{max} u_p \right)^2. \qquad (37)$$

This quantity depends on the energy of each short pulse u_p, but it does not depend on the number of pulses n and their total energy U.

Numerical evaluations can differ by many orders of magnitude, since different authors gave rather different values of the surface second order nonlinear coefficients for the diamond. A model considered in [17] resulted in the values of $\tilde{\chi}^{(2)}$ up to $10^{-20}\,\mathrm{m}^2/\mathrm{V}$ in the SI units, while experimental data given in [18] corresponded to the values from $10^{-26}\,\mathrm{m}^2/\mathrm{V}$ to $6 \times 10^{-24}\,\mathrm{m}^2/\mathrm{V}$. To transform these values to the Gaussian units one has to multiply them by the factor $3 \times 10^4/(4\pi)$ [15]. We take the value $\tilde{\chi}^{(2)}_{max} = 10^{-15}$ in the Gaussian units for the most pessimistic evaluation. The crystal used in our experiments had the volume about $20\,\mathrm{mm}^3$ (see the next section). For the cavity scaled by the factor of 30 this volume should be about $10^{-6}\,\mathrm{cm}^3$, and the cavity frequency ω_c should be about $5 \times 10^{11}\,\mathrm{s}^{-1}$. Thus we get $\mathcal{N}^{(2)}_{max} \sim 5 \times 10^{-3}$ for $\varepsilon = 5$ and $u_p = 2\,\mu\mathrm{J}$. Hence it seems that the surface effects are not dangerous for ideal crystals like diamond. Nonetheless, if the bulk $\chi^{(2)}$ coefficient is different from zero (e.g., due to some defects), then the number of spurious photons can be not so small. In the next section we present the results of experiments aimed at the study of the RF radiation generated in a cavity containing crystals with nonzero $\chi^{(2)}$ bulk coefficients.

3. Experimental apparatus

In this section we describe the experimental apparatus, schematized in Fig. 2, that has been used to investigate possible spurious, $\chi^{(2)}$-related effects in a DCE experiment based on the modulation of the index of refraction of a nonlinear crystal. We remark that detectable $\chi^{(3)}$-related parametric amplification effects are not expected in the present apparatus, that is characterized by a combination of parameters (cavity frequency of resonance and gap size, laser repetition rate, choice of the crystal) not adequate to satisfy the requirements described in section 2.3.

3.1. The microwave cavity

The heart of our experimental scheme, shown in Fig. 2, is a copper reentrant cylinder cavity. Its dimensions are $H = 26.2$, $D = 38$ and $h = 22.8$, $d = 6$ respectively external and internal cylinder height and diameter in mm. The reentrant part of the cavity is composed of a cylinder and of a cone to further concentrate the field lines in the gap, as shown in Fig. 3, where the nonlinear crystal under test can be set. The displayed magnetic and electric field profiles of the lowest frequency TM_{010} mode that we considered have been obtained through numerical simulations based on

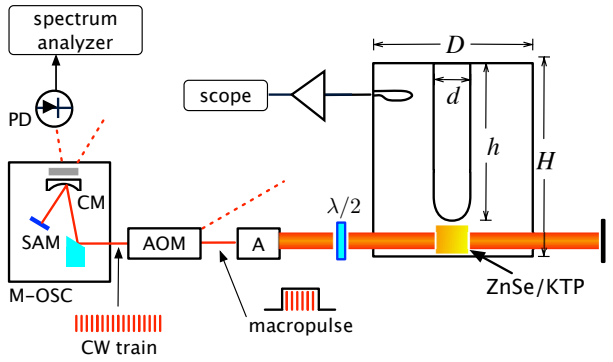

Figure 2. Scheme of the experimental apparatus. The laser master oscillator (M-OSC) delivers a CW train of infrared pulses. An AOM selects a finite number of pulses to be amplified in A, a double stage optical amplifier. The ultrafast photodiode PD detects the loss of the curved mirror CM to monitor the laser pulses repetition rate. A reentrant cylinder cavity hosts the nonlinear crystal (ZnSe or KTP). Its dimensions are: $H = 26.2$, $D = 38$ and $h = 22.8$, $d = 6$ respectively external and internal cylinder height and diameter in mm.

the finite element method (FEM).

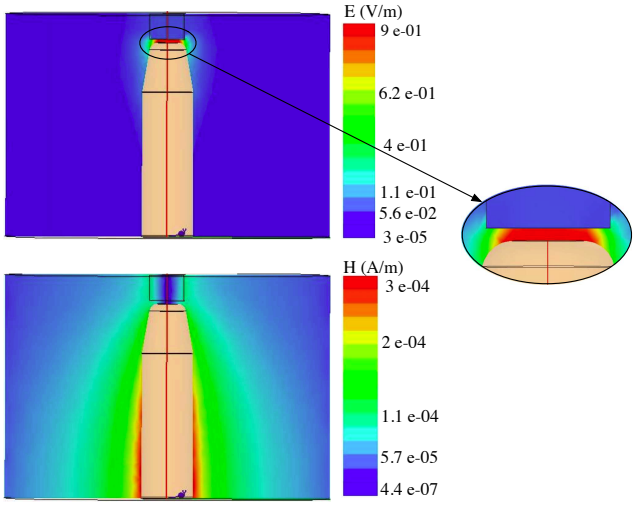

Figure 3. Electric (up) and magnetic (down) field profile in the reentrant cylinder cavity used. The reentrant part of the cavity is composed of a cylinder and a cone, whose smaller diameter (on the crystal side) is of 4 mm.

The loaded cavity quality factor $Q_L = f_c/\Delta f$, where Δf is the cavity linewidth, is about 2500 but the non null tangent loss ($\tan\delta$) of crystals can significantly degrade it. For instance, with ZnSe ($\tan\delta = 0.0017$ at room temperature) we measured $Q_L = 860$.

Light can be made to directly impinge on the nonlinear crystal through an aperture whose diameter is comparable with the laser beam waist. Opposite to the entrance hole, an equivalent aperture allows light to exit the cavity. Field amplitudes in the cavity are measured through a coaxial transmission line ended by an inductive loop coupled to the cavity mdoe. A 33 dB gain Miteq microwave amplifier is used to amplify the microwave signals to a level greater than the noise floor of a high-rate sampling digital oscilloscope (6 GHz bandwidth).

3.2. The laser oscillator

Stable emission of laser pulses at high repetition rate is a necessary requirement to satisfy the parametric resonance condition in a 3D microwave cavity and can be obtained from passively mode-locked lasers [34].

In the present work we use a multi-GHz passively mode-locked Nd:YVO_4 laser (M-OSC, master oscillator) that has been described elsewhere [35]. Its repetition rate can be changed in the interval $4.6 \leq f_l \leq 4.7$ GHz by properly adjusting the position of the curved mirror (CM) and of the saturable absorbing mirror (SAM) shown in Fig. 2. As the M-OSC output pulse energy ($\approx$ 5 pJ) is not sufficient to induce significant changes of the dielectric properties in a few cubic square millimeters nonlinear crystal, several amplification stages (diode-pumped Nd:YVO_4 and Nd:YAG flash-lamp pumped modules) are employed in order to enhance the pulse energy up to 10 μJ at 1064 nm wavelength. The amplified, 10 ps-long pulses are delivered in groups of $N \approx 2000$ pulses, separated by $t_l = 1/f_l \approx 200$ ps, so as to form 500 ns-long pulse trains that can be repeated once per second.

A source of spurious photons in a DCE experiment is due to the finite duration of the train of laser pulses. In fact, in the frequency domain the pulses train can be represented by a series of regularly spaced harmonics (the principal maxima) at frequencies $f_m = mf_l$, integer multiples of the fundamental frequency f_l. The width of each harmonic is set by the duration of the macro pulse T_t. If for simplicity we consider rectangular pulses, the harmonics amplitude decreases with increasing order, in much the same way as the amplitude of the principal maxima in the interference figure obtained with a diffraction grating made of rectangular slits. The envelope A_m of the amplitude of the principal maxima in this case is given by

$$A_m = \left| \frac{\sin 2\pi m f_l \tau}{2\pi m f_l \tau} \right| \tag{38}$$

where $\tau = 10$ ps is the duration of each individual pulse in the train. Note that $N-1$ secondary maxima appear between the harmonics and can be observed as side lobes surrounding each principal maximum, as can be noted in the central part of Fig. 4, where the spectrum of a macro pulse consisting of $N = 2000$, 10 ps-long, rectangular pulses is displayed. In inset (a) we show the envelope of all maxima, i.e., including the secondary ones, of the diffraction-like spectrum for the first two harmonics of the train. It has been

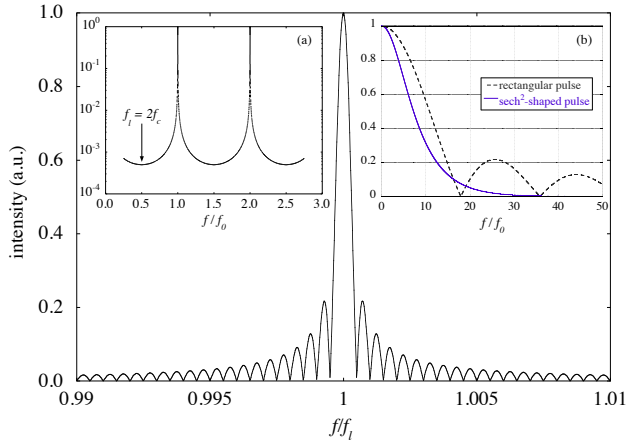

Figure 4. Optical pulses in the frequency domain. A train of pulses has a spectrum composed of several harmonics whose relative amplitude is determined by the single pulse shape. When a finite number of pulses is considered, secondary maxima are observed between each harmonic, as shown in the central part of the figure. In inset (a) we show the first two harmonics and indicate the secondary maxima floor at the condition of parametric resonance ($f_l = 2f_c$), calculated for the macro pulse employed in the present work. The difference between trains of rectangular and squared hyperbolic secant (sech) pulses of 10 ps duration, separated by approximately 200 ps ($f_l = 5$ GHz), is displayed in inset (b).

calculated for the macro pulse duration we used during the present measurements ($N = 2000$, $\Delta t \sim 450$ ns). For DCE esxperiments, it is important to note that at the cavity frequency $f_c = f_l/2$, the secondary maxima envelope establishes a floor at the level of 10^{-3}, which can be relevant for the generation of $\chi^{(2)}$-related photons. A cw pulsed laser excitation would instead produce a sequence of perfectly isolated harmonics. Unfortunately, there are no mode-locked oscillators that can deliver in CW the requested laser/energy per pulse, and we need to optically select and amplify only a finite number of pulses.

For the sake of completeness we also report in inset (b) of Fig. 4 the resulting harmonics envelope when the actual optical pulse is considered, whose temporal profile is given by a squared hyperbolic secant. Such profile yields an envelope that differs from the rectangular shape considered in Fig. 4 (a), even though the difference between the two envelopes for the first few harmonics is hardly detectable.

Up to now we have considered an ideal oscillator, and identified the finite train duration as a possible source of spurious photons in DCE experiments. However, the actual spectrum of our mode-locked oscillator can significantly differ from the ideal situation, as shown in the example in Fig. 5, and the influence of unwanted secondary oscillations of the laser source must also be considered. For instance, in addition to $f_l \approx 4.6$ GHz and the second harmonic $2f_l$ of the train of pulses, secondary oscillations at $f_{1,2} < f_l$ emerge in the spectrum, that modulate the carrier frequency f_l and that in turn appear as sidebands to each harmonic of the train.

Table 1. Second- and third-order nonlinear optical coefficients of selected materials [42].

Material	n_2 (cm^2/W)	$\chi^{(3)}$ (esu)	d (pm/V)
diamond	$1.3 \cdot 10^{-15}$	$1.8 \cdot 10^{-13}$	
GaAs	$3.3 \cdot 10^{-13}$	$1.0 \cdot 10^{-10}$	$d_{14} = 90.4$
ZnSe	$3 \cdot 10^{-14}$	$4.4 \cdot 10^{-12}$	$50 - 60$

In order to obtain a laser spectrum characterized by the smallest secondary oscillations, tiny adjustments of the master oscillator curved mirror and the SAM are performed while observing its photodiode signal at a spectrum analyzer (Agilent ESA-E E4405B). We note that to thoroughly suppress unwanted secondary oscillations, some Q-switching instabilities necessarily arise around the carrier, as proved for several M-OSC different alignments and f_l frequencies. In Fig. 5 (b) the relaxation oscillations ($f_{rx}^{\pm} \sim f_l \pm 3$ MHz) in the spectrum of our passively mode-locked laser oscillator are also shown. These oscillations are in general considered acceptable when their amplitude is at least 30 dB smaller than that of the carrier [37]. Until now, there have been many reports of noise measurements on mode-locked lasers [39–41], but almost always the power density of phase noise up to a few MHz is reported, whereas the secondary oscillations we observe occur at a much higher frequency, from a few hundreds MHz to approximately 2 GHz. In the present work we maintain the cleanest mode locking condition, whereby both the secondary peaks and the relaxation oscillations are kept at least 40 dB below the amplitude of the carrier frequency f_l. Once this condition is met, the master oscillator repetition rate is locked to a microwave oscillator by means of a feedback circuit described elsewhere [38] and is thus stabilized during the measurements.

3.3. The nonlinear crystal

As described in section 2, high speed switching boundary conditions to the EM field can be realized by exploiting the intensity dependent refractive index $n = n_0 + n_2 I$, where I is the laser intensity and n_2 is related to the nonlinear susceptibility by means of [15]

$$n_2 = 12\pi^2 \chi^{(3)}/n_0^2. \tag{39}$$

Therefore a primary requirement is to find a material, in which $\chi^{(3)}$ is sufficiently large. Semiconductors often possess a large third order susceptibility, typically in the range $10^{-13} - 10^{-10}$ esu, while insulating solids are characterized by a nonlinear coefficient $\chi^{(3)}$ of the order of $10^{-13} - 10^{-14}$ [42]. Eq. (39) applies both to

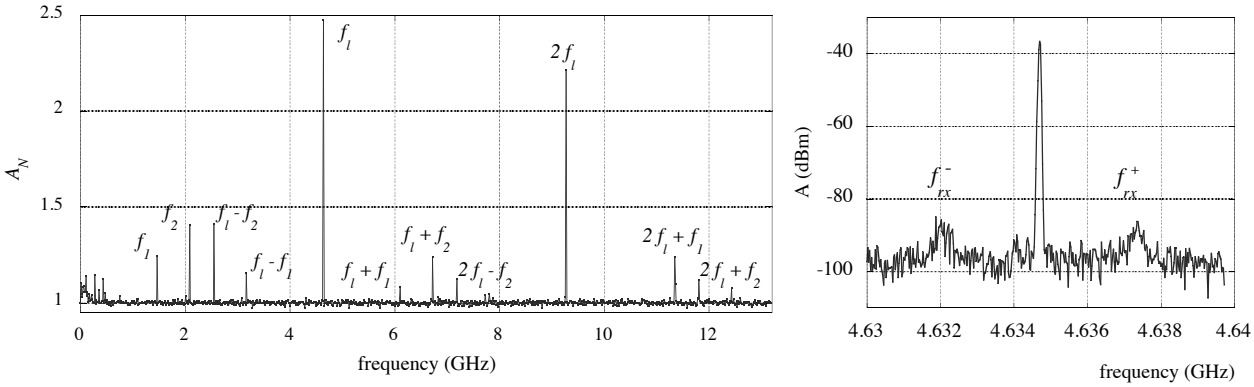

Figure 5. Representative spectrum of the master oscillator acquired by a fast photodetector with bandwidth greater than 15 GHz (EOT InGaAs pin detector ET-3500). The spectrum extends up to 13.2 GHz, the upper frequency of the spectrum analyzer. The displayed amplitudes A_N are obtained by means of dividing the logarithmic amplitudes observed in the optical signal spectrum by the noise floor of the spectrum analyzer. Secondary oscillations, in addition to the first and second harmonic of the train of pulses (respectively f_l and $2f_l$), are indicated by f_1 and f_2. Since these frequencies represent a modulation of the intensity of the train of pulses delivered by the master oscillator, they also appear as sidebands ($f_l \pm f_{1,2}$) to each harmonic. It is worth noticing that the amplitude of the peaks at $f_{1,2}$ is more than 30 dB smaller than the carrier frequency at f_l. On the right side our typical level of the relaxation oscillations $f_{rx}^{\pm}$ is shown (50 dB smaller than the first harmonic peak amplitude), acquired with 30 kHz resolution bandwidth.

a semiconductor and an insulating solid as diamond for an incident photon energy smaller than the band gap energy. In Table 1 we report values of $\chi^{(3)}$, n_2 and the scalar second order nonlinear coefficient d for some materials that we considered. The most attractive material for such type of experiment appears to be a semiconductor (GaAs), whose $\chi^{(3)}$ is nearly two orders of magnitude greater than in diamond, the latter being used in many nonlinear optics applications [19, 43]. However, we point out that infrared photon ($\lambda = 1064\,\text{nm}$) absorption was observed in semi-insulating GaAs, and this limits the possibility to use it in our experiment, in which laser-excited carriers, responsible of ohmic losses for the cavity microwave field, are not allowed [44]. Absorption of photons with energy smaller than the band gap is in fact possible through the $EL2-$like defect [45]. In Table 1 we also report the properties of ZnSe (zinc selenide), another semiconductor belonging to the zinc-blende II-IV group whose band gap is 2.7 eV at room temperature.

In the following sections we report measurements carried out with ZnSe and KTP crystals.

4. Measurement results

4.1. Measurements with a KTP crystal

To better understand the role of the second order nonlinear coefficient in the DCE experiment, we have mounted in the cavity gap a potassium titanyl phosphate ($KTiOPO_4$, KTP) crystal, a material that is being widely used for several second-order nonlinear optical applications due to its high nonlinear d coefficient [46].

The KTP $\chi^{(2)}$-related photons emitted at frequency f_l have been studied in a previous work with a cavity receiver at $f_c \sim f_l$ [21]. The amount of generated radiation has been demonstrated to be so high that amplification was not needed and few hundred mV signals were recorded at the oscilloscope with $\sim 70\,\text{MW/cm}^2$ laser pulse intensity. Here we study the KTP $\chi^{(2)}$-related photons detected in a DCE cavity with $f_c \sim f_l/2$. To establish a direct experimental link between the cavity field and the infrared laser spectra, we mount the device described in Ref. [36] on the beam line before the cavity entrance. This device allows acquisition of the spectrum of the KTP $\chi^{(2)}$-related radiation without the bandwidth limitations of the cavity. The inner and outer diameters of its coaxial structure are such that the TEM mode cutoff frequency is approximately 8.5 GHz.

When the laser pulse impinges in the KTP crystal set in the cavity gap, we observe *modulated* microwave pulses, as shown in Fig. 6 for a set of six different laser repetition rate values. The train of pulses starts at $t = 0$ and lasts for an interval of 500 ns, during which a modulated microwave field is observed. Afterwards the energy stored in the cavity exponentially decays with the cavity time constant $\tau_L \sim 200\,\text{ns}$.

Simultaneous acquisition of the corresponding signal spectra in the wide-bandwidth coaxial device are reported in Fig. 7. We observe that if unwanted frequency peaks f_i and the coupled f_j in the infrared laser train spectrum appear in the vicinity of f_c, they can beat and give rise to modulated pulses. In fact, the period of the modulation in each panel of Fig. 6 corresponds exactly to the inverse of the frequency

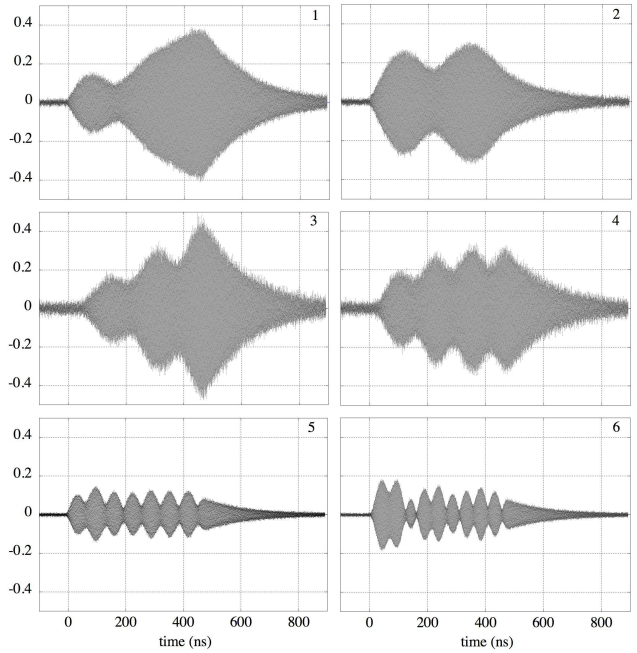

Figure 6. Modulated microwave pulses detected in the cavity for a few different master oscillator alignments. The laser excitation starts at instant 0 and lasts approximately 500 ns. Exponential decay of the stored field is afterwards observed. The repetition rate of the pulses f_l was set to 1 = 4.6766 GHz; 2 = 4.6767 GHz; 3 = 4.67685 GHz; 4 = 4.677 GHz; 5 = 4.6761 GHz; 6 = 4.6776 GHz.

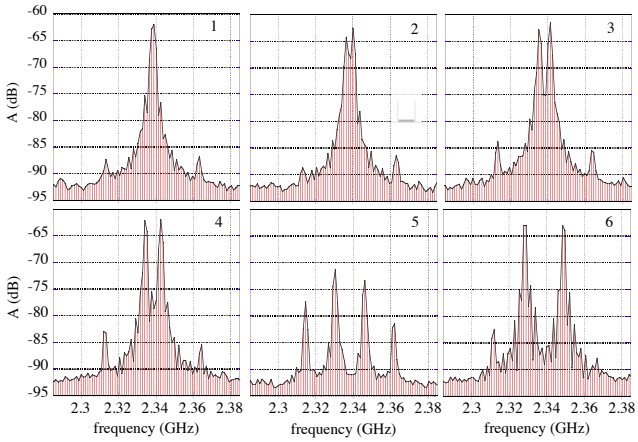

Figure 7. Coaxial structure wide-bandwidth detection. The master oscillator secondary oscillations f_i and $f_j = f_l - f_i$, detected in the master oscillator microwave spectrum in the vicinity of $f_c = 2.33525$ GHz (central frequency of each plot). Their corresponding frequency is resolved to the best of 2 MHz, due to the macro pulse duration ($T_t = 500$ ns). For this reason f_i and f_j are not resolved in the first plot. In plot number 5 additional frequencies are observed, but they do not influence the corresponding plot in Fig. 6 because they are too far from the cavity resonance.

difference of the peaks in Fig. 7, as resumed in Table 2. Note that the frequency resolution cannot be better than 2 MHz due to the finite duration $T_t \sim 500$ ns of the train and thus the detected secondary oscillations f_i and the coupled f_j cannot be resolved when they are very close (see for instance Fig. 7 (1)).

Table 2. Identification of the pulsed microwave radiation observed with the KTP crystal. In the first column we report the value of the laser repetition rate that characterizes each alignment as described in the caption of Fig 6; $f_{i,j}$ are the frequencies of the secondary oscillations detected in the master oscillator spectra displayed in Fig. 7. T is the period of the modulation measured from the microwave pulses in Fig. 6.

	f_l (GHz)	T^{-1} (MHz)	f_i (GHz)	f_j (GHz)	$f_i - f_j$ (MHz)
1	4.6766	$\sim 1/T_t$	–	–	$\leqslant 2$
2	4.6767	4.4±0.4	2.3365	2.3402	3.7
3	4.67685	6.6±0.6	2.3352	2.3413	6.1
4	4.677	8.7±0.7	2.3338	2.3427	8.9
5	4.6761	15.6±0.3	2.3305	2.3462	15.7
6	4.6776	20.5±0.6	2.3285	2.3492	20.7

Finally, when secondary oscillations are not detected in the vicinity of the cavity, the microwave signal detected in the cavity is small, and presents an instantaneous rise and no exponential decay of the stored field at the end of the laser excitation. This signal is investigated in detail in the following section with the ZnSe crystal.

4.2. Measurements with a ZnSe crystal

The ZnSe crystal used is a parallelepiped $3 \times 3 \times 2\,\mathrm{mm}^3$ in size whose short axis is aligned along the direction of laser propagation (x axis). The signal in Fig. 8 is observed when at $t = 0$ a train of laser pulses with total energy $U = 70.2$ mJ impinges on the ZnSe crystal. As the laser beam gaussian diameter at the crystal position is of approximately 2 mm, the pulse intensity is $\sim 100\,\mathrm{MW/cm}^2$. To understand the physical origin of such signal, which can be a relevant source of spurious photons in DCE experiments, in the lower part of Fig. 9 we plot the spectrum of the microwave signal of Fig. 8, obtained by averaging over 100 signal FFTs (Fast Fourier Transform) calculated for each signal. The cavity data are supplemented with the spectrum of the laser master oscillator, shown in the upper part of the Fig. 9. The laser oscillator repetition rate is set to $f_l = 4.6347$ GHz and the displayed optical signal FFT is obtained as described in section 3.2. In the optical spectrum of the M-OSC several secondary oscillations ($f_{3,4}$ and the coupled $f_{3,4} - f_l$) are detected, whereas the microwave signal in the cavity displays only f_4 and its coupled frequency $f_l - f_4$. Note that the cavity linewidth is 2.7 MHz, and that $|f_c - f_{3,4}| \geqslant 200$ MHz. By varying the MOSC alignment conditions (as shown, for instance, in Fig. 10), we observed that the area under the peak at f_c is roughly independent of the

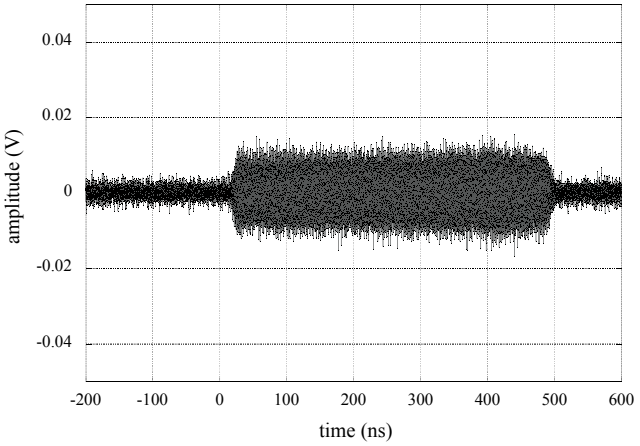

Figure 8. Microwave signal detected in the cavity. The train of pulses impinges on the ZnSe crystal at $t = 0$ and lasts approximately 500 ns. The optical pulse intensity is $\sim 100\,\mathrm{MW/cm^2}$.

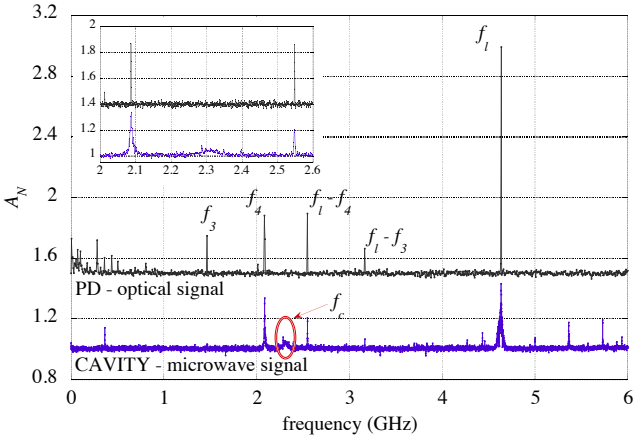

Figure 9. Laser oscillator spectrum (indicated by the label "PD - optical signal") and frequency analysis of the signal detected in the cavity up to 6 GHz (CAVITY - microwave signal). Both the spectra are normalized to the respective noise floors of the instruments used (the spectrum analyzer and the oscilloscope), as described in detail in the text. The laser oscillator repetition rate was set to $f_l = 4.6347$ GHz. In the inset, both spectra are shown around f_c, to evidence that there are no laser oscillations at the cavity frequency of resonance. The spectrum analyzer was set to 30 kHz resolution bandwidth. The M-OSC spectrum has been upwards shifted for visibility purposes.

oscillator spectrum. We believe that this signal is of electronic origin, a crosstalk between the cavity and the amplifier input that could possibly be reduced using a much higher quality factor cavity resonator.

5. Discussion and conclusions

In this work we have studied both theoretically and experimentally the parametric excitation of a microwave cavity resonator with of a train of multi-

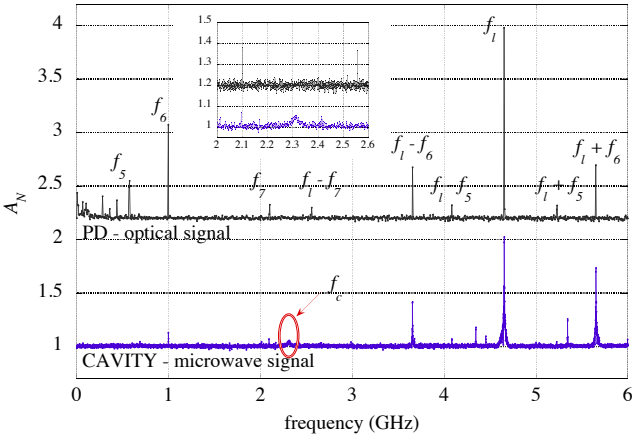

Figure 10. Data are displayed as in Fig. 9 for a different master oscillator configuration, whose repetition rate was in this case set to $f_l = 4.6552$ GHz. As compared to the previous oscillator alignment, in the laser spectrum much smaller secondary oscillations around f_c (f_7 and its mirrored $f_7 - f_l$) are displayed. Secondary oscillations $f_{5,6}$ at a smaller frequency than those observed in the previous example are in this alignment detected.

GHz laser pulses acting on a nonlinear crystal enclosed within the cavity itself. Our final aim is to establish the suitable experimental conditions to study the DCE in the three dimensional case.

In section 2 we have estimated the number of photons that can be generated inside the cavity, starting from the vacuum state of the electromagnetic field, through excitation of the third order nonlinear response of the crystal, proportional to $\chi^{(3)}$. An optimized cavity (and nonlinear crystal) geometry has been proposed, which requires a much higher repetition rate laser system (and, as a consequence, a smaller cavity) than the one implemented in the preliminary measurements reported in the second part of the present work. Nonetheless, the non-optimized scheme enables us to investigate possible spurious effects in dynamical Casimir experiments. We singled out three different processes of spurious photon generation. The first one, studied theoretically in section 2.4, is related to the evaluation of the maximal possible number of the spurious RF quanta, generated by periodical laser pulses, whose influence can be described within a simple model of an oscillator, excited by a classical force proportional to the $\chi^{(2)}$ nonlinear coefficients.

The second one, described in section 3.2, is related to the finite duration of the optical excitation and it can be reduced by increasing the laser excitation duration. We ought to consider here that in principle the laser pulses cannot have exactly the same energy, thereby creating a quantum noise floor between the main peaks at $f_m = mf_l$ also in the case of a cw laser excitation [47].

Both in the first and the second issues the laser oscillator is considered to be ideal (i.e. the laser spectrum contains only the harmonics f_m). The third problem is instead related to the actual oscillator, that can exhibit secondary oscillations in the vicinity of the cavity resonance, and its influence has been experimentally studied in section 4.1. We have seen that a very small modulation of the infrared train of pulses intensity (the level of the detected secondary oscillation $f_{i,j}$ is found to be more than 30 dB less than the carrier frequency f_l) is a direct source of microwave photons. The effect is related to the second order coefficient d of the nonlinear crystal, in which a time-dependent polarization is produced as a consequence of optical rectification (OR) [21]. Due to this phenomenon, the crystal behaves as if it were an antenna that radiates an electromagnetic field whose frequency content is directly related to the laser spectrum. Therefore any optical frequency component is to be regarded as a generation of photons inside the cavity. We remark the fact that any optical crystal is characterized by a second order nonlinearity. Therefore, regardless how small it is, its role has to be considered in the QED experiment.

Finally, both with a KTP and a ZnSe crystal, even if the secondary oscillations near the cavity resonance are reduced below our receiver sensitivity, a spurious signal is detected, whose shape suggests its possible origin, i.e. a cross-talk between the cavity and the amplifier input. A higher quality factor cavity could be of help to reduce this noise. Moreover, we expect an improved detection scheme from the point of view of electronic noise when the cavity and a low noise amplification stage are both cooled to liquid helium temperatures, as demonstrated in Ref. [49]. In addition, at this temperature the number of thermal photons $kT/h\nu$ in the cavity mode is also very small, necessary condition to start a DCE experiment.

Acknowledgements

C. B. gratefully acknowledges the financial support of the University of Padova under Progetto di Ateneo (cod. CPDA135499/13). V. V. D. acknowledges a partial support from the Brazilian agency CNPq and the Visiting Professor grant from the University of Padova. The authors acknowledge the technical assistance of E. Berto from the University of Padova and INFN.

References

[1] Dodonov V V 2010 Current status of the dynamical Casimir effect *Phys. Scr.* **82** 038105

[2] Dalvit D A R, Maia Neto P A and Mazzitelli F D 2011 Fluctuations, dissipation and the dynamical Casimir effect, *Casimir Physics* (*Lecture Notes in Physics Vol 834*) ed D Dalvit, P Milonni, D Roberts and F da Rosa (Berlin: Springer) p 419–57

[3] Nation P D, Johansson J R, Blencowe M P and Nori F 2012 Stimulating uncertainty: Amplifying the quantum vacuum with superconducting circuits *Rev. Mod. Phys.* **84** 1–24

[4] Yablonovitch E 1989 Accelerating reference frame for electromagnetic waves in a rapidly growing plasma: Unruh–Davies–Fulling–De Witt radiation and the nonadiabatic Casimir effect *Phys. Rev. Lett.* **62** 1742–5

[5] Yablonovitch E, Heritage J P, Aspnes D E and Yafet Y 1989 Virtual photoconductivity *Phys. Rev. Lett.* **63** 976–9

[6] Lobashov A A and Mostepanenko V M 1991 Quantum effects in nonlinear insulating materials in the presence of a nonstationary electromagnetic field *Teor. Mat. Fiz.* **86** 438–47 [*Theor. & Math. Phys.* **86** 303–9]

[7] Lobashov A A and Mostepanenko V M 1991 Quantum effects associated with parametric generation of light and the theory of squeezed states *Teor. Mat. Fiz.* **88** 340–57 [*Theor. & Math. Phys.* **88** 913–25]

[8] Hizhnyakov V V 1992 Quantum emission of a medium with a time-dependent refractive index *Quant. Opt.* **4** 277–80

[9] Hizhnyakov V and Kaasik H 2005 Emission by dielectric with oscillating refractive index *J. Phys.: Conf. Ser.* **21** 155–60

[10] Dezael F X and Lambrecht A 2010 Analogue Casimir radiation using an optical parametric oscillator *EPL* **89** 14001

[11] Faccio D and Carusotto I 2011 Dynamical Casimir Effect in optically modulated cavities *EPL* **96** 24006

[12] Schützhold R 2011 Refractive index perturbations – Unruh effect, Hawking radiation or dynamical Casimir effect? e-print arXiv:quant-ph/1110.6064

[13] Hizhnyakov V, Kaasik H and Tehver I 2014 Spontaneous nonparametric down-conversion of light *Appl. Phys.* A **115** 563–8

[14] Dodonov V V 2015 Dynamical Casimir effect in microwave cavities containing nonlinear crystals *J. Phys.: Condens. Matter* **27** 214009

[15] Boyd R W 2003 *Nonlinear Optics* (San Diego: Academic)

[16] Sipe J E, Moss D J and van Driel H M 1987 Phenomenological theory of optical second- and third-harmonic generation from cubic centrosymmetric crystals *Phys. Rev.* B **35** 1129–41

[17] Gavrilenko V I and Rebentrost F 1995 Nonlinear optical susceptibility of the surfaces of silicon and diamond *Surf. Sci.* **331-3** 1355–60

[18] Schliesing R, Eichhorn G, Jiang X and Zacharias H 1997 The complex tensor components of the nonlinear susceptibility $\chi^{(2)}$ of C(100) and of the C/Si(100) interface *Surf. Sci.* **387** 279–87

[19] Trojánek F, Žídek K, Dzurňák B, Kozák M and Malý P 2010 Nonlinear optical properties of nanocrystalline diamond *Opt. Express* **18** 1349–57

[20] Schriever C, Bianco F, Cazzanelli M, Ghulinyan M, Eisenschmidt C, de Boor J, Schmid A, Heitmann J, Pavesi L and Schilling J 2015 Second-order optical nonlinearity in silicon waveguides: inhomogeneous stress and interfaces *Adv. Optical Mater.* **3** 129–36

[21] Borghesani A F, Braggio C and Carugno G 2013 Generation of microwave radiation by nonlinear interaction of a high-power, high-repetition rate, 1064 nm laser in $KTiOPO_4$ crystals *Opt. Lett.* **38** 4465–8

[22] Borghesani A F, Braggio C and Guarise M 2016 Microwave emission by nonlinear crystals irradiated with a high-intensity, mode-locked laser *J. Opt.* **18** 065503

[23] Simon R, Sudarshan E C G and Mukunda N 1986 Gaussian–Maxwell beams *J. Opt. Soc. Am.* A **3** 536–40

[24] Dodonov V V and Klimov A B 1996 Generation and

detection of photons in a cavity with a resonantly oscillating boundary *Phys. Rev.* A **53** 2664–82
[25] Dodonov A V and Dodonov V V 2012 Dynamical Casimir effect in a cavity with a weakly non-equidistant spectrum *Phys. Lett.* A **376** 1903–6
[26] Dodonov V V and Dodonov A V 2016 Excitation of the classical electromagnetic field in a cavity containing a thin slab with a time-dependent conductivity *J.Russ. Las. Res.* **37** 107–22
[27] Dodonov A V, Dodonov E V and Dodonov V V 2003 Photon generation from vacuum in nondegenerate cavities with regular and random periodic displacements of boundaries *Phys. Lett.* A **317** 378–88
[28] Dodonov A V and Dodonov V V 2005 Resonance generation of photons from vacuum in cavities due to strong periodic changes of conductivity in a thin semiconductor boundary layer *J. Opt. B: Quantum Semiclassical Opt.* **7** S47–58
[29] Dodonov V V 2011 Quantum damped nonstationary oscillator and dynamical Casimir effect *Revista Mexicana de Física* **S57** 120–7
[30] van Bladel J 1964 *Electromagnetic Fields* (New York: McGraw-Hill) Chap. 10
[31] Landau L D, Lifshitz E M and Pitaevskii L P 1984 *Electrodynamics of Continuous Media* (Amsterdam: Elsevier) Sec. 90
[32] Dodonov V V 2010 Approximate formulas for the resonance frequency shift in cavities with big variations of parameters inside small regions *Phys. Rev.* A **82** 043808
[33] Padamsee H, Knobloch J and Hays T 2008 *RF Superconductivity for Accelerators* (Wiley-VCH)
[34] Keller U 2003 Recent developments in compact ultrafast lasers *Nature* **424** 831–8
[35] Agnesi A, Braggio C, Carrà L, Pirzio F, Lodo S, Messineo G, Scarpa D, Tomaselli A, Reali G and Vacchi C 2008 Laser system generating 250-mJ bunches of 5-GHz repetition rate, 12-ps pulses *Opt. Express* **16** 15811–5
[36] Braggio C and Borghesani A F 2014 A contactless microwave-based diagnostic tool for high repetition rate laser systems *Rev. Sci. Instrum.* **85** 023105
[37] Schlatter A, Zeller S C, Grange R, Paschotta R and Keller U 2004 Pulse-energy dynamics of passively mode-locked solid-state lasers above the Q-switching threshold *J. Opt. Soc. Am. B* **21** 1469–78
[38] Agnesi A, Braggio C, Carugno G, Della Valle F, Galeazzi G, Messineo G, Pirzio F, Reali G and Ruoso G 2011 A laser system for the parametric amplification of electromagnetic fields in a microwave cavity *Rev. Sci. Instrum.* **82** 115107
[39] von der Linde D 1986 Characterization of the noise in continuously operating mode-locked lasers *Appl. Phys. B* **39** 201–17
[40] Haus H A and Mecozzi A 1993 Noise of mode-locked lasers *IEEE J. Quantum Electron.* **29** 983–96
[41] Paschotta R 2004 Noise of mode-locked lasers (Part I): numerical model *Appl. Phys. B* **79** 153–62
[42] Boyd R W and Fischer G L 2001 *Encyclopedia of Materials: Science and Technology* (Amsterdam: Elsevier)
[43] Faccio D, Arane T, Lamperti M and Leonhardt U 2012 Optical black hole lasers *Class. Quantum Grav.* **29** 224009
[44] Braggio C, Carugno G, Della Valle F, Ruoso G and Zanello D In preparation
[45] Manasreh M O, Look D C, Evans K R and Stutz C E 1990 Infrared absorption of deep defects in molecular-beam-epitaxial GaAs layers grown at 200 °C: Observation of an $EL2$-like defect *Phys. Rev. B* **41** 10272–5
[46] Bierlein J D and Vanherzeele H 1989 Potassium titanyl phosphate: properties and new applications *J. Opt. Soc. Am. B* **6** 622–33
[47] Bachor H A and Ralph T C 2004 *A Guide to Experiments in Quantum Optics* (Wiley-VCH)
[48] Dowling J P, Scully M O and De Martini F 1991 Radiation pattern of a classical dipole in a cavity *Optics Comm.* **82** 415–9
[49] Braggio C, Bressi G, Carugno G, Della Valle F, Galeazzi G and Ruoso G 2009 Characterization of a low noise microwave receiver for the detection of vacuum photons *Nucl. Instrum. and Meth. A* **603** 451–5